Inorganic Chemistry

Article

pubs.acs.org/IC

Design and Synthesis of an MOF Thermometer with High Sensitivity in the Physiological Temperature Range

Dian Zhao, Xingtang Rao, Jiancan Yu, Yuanjing Cui,* Yu Yang, and Guodong Qian*

State Key Laboratory of Silicon Materials, Cyrus Tang Center for Sensor Materials and Applications, School of Materials Science and Engineering, Zhejiang University, Hangzhou 310027, P. R. China

Supporting Information

ABSTRACT: An important result of research on mixed-lanthanide metal−organic frameworks (M′LnMOFs) is the realization of highly sensitive ratiometric luminescent thermometers. Here, we report the design and synthesis of the new M′LnMOF $Tb_{0.80}Eu_{0.20}BPDA$ with high relative sensitivity in the physiological temperature regime (298−318 K). The emission intensity and luminescence lifetime were investigated and compared to those of existing materials. It was found that the temperature-dependent luminescence properties of $Tb_{0.80}Eu_{0.20}BPDA$ are strongly associated with the distribution of the energy levels of the ligand. Such a property can be useful in the design of highly sensitive M′LnMOF thermometers.

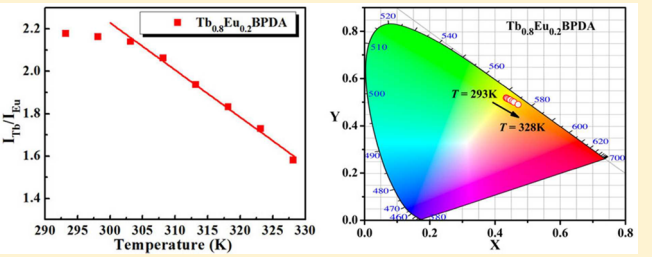

INTRODUCTION

Luminescence-based thermometers have attracted much attention because of their unique characteristics: noninvasiveness, accuracy, fast response, high spatial resolution, and applicability even under strong electromagnetic fields and rapidly changing conditions.[1] Temperature-dependent fluorescent properties, such as changes in energy,[2] lifetime,[3] and intensity,[4] have been used as the main metrics in temperature measurements and sensing. However, for measurements of energy variations and luminescence lifetimes, relatively long times and postprocessing computational treatment are required. Moreover, measurements based on a single transition intensity can be affected by variations in the sensor concentration, material inhomogeneity, or excitation power, as well as drifts within the optoelectronic system, such as lamps and detectors. These drawbacks often reduce the accuracy and restrict the general utility of these techniques. In contrast, ratiometric, or self-calibrating, intensity measurements can avoid these drawbacks and are very reliable for precise temperature sensing.[5] To date, several luminescent materials have been explored and developed as ratiometric thermometers. These include molecular lanthanide coordination compounds, semiconducting polymer dots, Eu^{3+}/Tb^{3+} codoped organic−inorganic hybrids, and Er^{3+}/Yb^{3+} codoped upconversion nanoparticles.[6]

More recently, mixed-lanthanide metal−organic frameworks (M′LnMOFs) have been receiving wide attention for use as ratiometric thermometers.[5,7,8b,9e] That is, MOFs self-assembled from metal ions and/or clusters with organic linkers can be modified by organic synthesis; they have geometrically well-defined structures in terms of dimensions, size, and shape;[8] and their luminescent properties can be modulated by deliberate selection of inorganic and organic building blocks.[9] Several ratiometric luminescent MOF thermometers have been synthesized using the M′LnMOF approach and demonstrated for the intensity ratio between the characteristic emissions of Tb^{3+} at 545 nm and Eu^{3+} at 613 nm, and an excellent linear correlation from 10 to 300 K was found.[5a,7c,d] However, materials and techniques for sensing in the physiological temperature range (298−318 K) or higher are still rare and worth exploring. It is well-known that ligands are crucial for the luminescence properties of M′LnMOFs, because of the different crystal structures formed by the ligands and Ln ions, as well as the interactions among them, including energy transfer, radiation, nonradiative mixed decay, and quenching.[9a,c] Thus, it is desirable and challenging to find new and better MOFs for the purpose of temperature sensing. We noticed that Cadiau et al.[7e] have put forward the ratiometric nanothermometer $Tb_{0.99}Eu_{0.01}(BDC)_{1.5}(H_2O)_2$ in the physiological temperature range with relative sensitivities of 0.31%/K and 0.14%/K in water and solid, respectively. However, higher sensitivity and more accurate sensing in the physiological temperature range are of urgent interest.

As is well-known, an organic ligand with a suitable triplet energy state in the range of 22000−27000 cm^{-1}, as the linker to construct the M′LnMOFs with Tb^{3+} and Eu^{3+} ions, can effectively sensitize Tb^{3+} and Eu^{3+} simultaneously, and the distribution of energy levels for the ligand is closely related to the energy-transfer process in the system.[7d,9a,c] We designed and synthesized a new ligand, namely, biphenyl-3,5-dicarboxylic acid (H_2BPDA), with a lowest triplet energy state of 25269 cm^{-1} and an appropriate energy-level distribution (calculated by time-dependent density functional theory), that can be used

Received: July 19, 2015

DOI: 10.1021/acs.inorgchem.5b01623
Inorg. Chem. XXXX, XXX, XXX−XXX

Scheme 1. Synthetic Route to the Organic Linker H_2BPDA Used to Construct LnBPDA

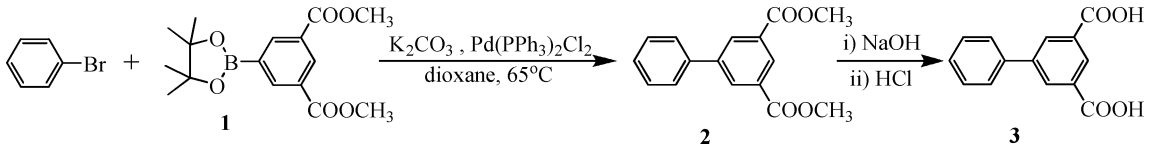

to fabricate the new M′LnMOFs. Accordingly, we synthesized $Tb_{0.80}Eu_{0.20}$BPDA, with a relative sensitivity 7.5 times larger than that of $Tb_{0.99}Eu_{0.01}(BDC)_{1.5}(H_2O)_2$[7e] at approximately 313 K, as a luminescent colorimetric thermometer applicable for in situ and real-time physiological temperature measurements.

EXPERIMENTAL SECTION

Materials and Measurements. All solvents and regeants were commercially available. ^{1}H NMR spectra were measured on a Bruker Advance DMX 500 spectrometer with an internal standard of tetramethylsilane (TMS). Thermogravimetric analysis (TGA) was performed using a Netzsch TG209F3 instrument at a heating rate of 5 °C/min under a N_2 atmosphere. Infrared (IR) spectra were obtained using a ThermoFisher Nicolet iS10 spectrometer with KBr pallets. Elemental analyses for C, H, and N were performed with an EA1112 microelemental analyzer. Powder X-ray diffraction (PXRD) patterns were measured using Cu Kα (λ = 1.542 Å) radiation on an X'Pert PRO diffractometer and recorded in the range of 2θ = 5−50° at room temperature. Room-temperature excitation and emission spectra for the samples were obtained on a Hitachi F4600 fluorescence spectrometer, with a photomultiplier tube voltage of 700 V; a scan speed of 4 nm/s; and slit widths of 2.5 and 1.5 nm, corresponding the excitation and emission spectra for H_2BPDA, and 1.0 and 1.0 nm for LnBPDA (Ln = Eu, Tb). The temperature dependence of the emission spectra and the luminescent decay curve were observed on an Edinburgh Instrument F920 spectrometer with the excitation wavelength of 323 nm; slits for both excitation and emission of 1.0 nm; and a peak count and channel of 5000 and 500, respectively.

Single-Crystal X-ray Diffraction. Single-crystal data were obtained on a Bruker Smart Apex II diffractometer equipped with graphite-monochromatized Mo Kα radiation (λ = 0.71073 Å) at 296 K and recorded on an Atlas detector. CryAlisPro was applied to determine the unit cells and collect the crystal data for EuBPDA. The data sets were corrected and implemented with the SCALE3 ABSPACK scaling algorithm,[10] and an empirical absorption correction using spherical harmonics was applied. Direct methods were applied to resolve the crystal structure, and the SHELX-2013 program package[11] on the basis of full-matrix least-squares method was used to refine the crystal structure. All non-hydrogen atoms and solvent molecules were located exactly and refined anisotropically on the basis of the Fourier maps. The hydrogen atoms on the ligands were generated geometrically, and the hydrogen atoms of the dimethylformamide (DMF) molecules were apparently visible in different maps and were handled with fixed isotropic displacement parameters in the subsequent refinement work. Crystallographic data are summarized in Table S1 (Supporting Information). CCDC 1400191 contains the supplementary crystallographic data for this article. These data are available from The Cambridge Crystallographic Data Centre at www.ccdc.cam.ac.uk/data_request/cif.

Computational Details. The molecular geometry optimization and frequency analysis of free ligands were performed using density functional theory (DFT) at the B3LYP/6-31+G(d,p) level,[12] and the optimized geometries and molecular orbital energies of free ligands are shown in Figure S15 (Supporting Information) and listed in Table S3 (Supporting Information). Based on the optimized results, the energies of the triplet excited states of the ligands were calculated by the time-dependent DFT approach,[13] and the results are reported in Table S3 (Supporting Information). All calculations were performed using Gaussian 09 software.[14]

Synthesis of the Organic Linker H_2BPDA. The synthesis route for H_2BPDA is shown in Scheme 1. Dimethyl 5-(4,4,5,5-tetramethyl-1,3,2-dioxaborolan-2-yl) isophthalate (**1**) was synthesized according to ref 15.

To prepare dimethyl biphenyl-3,5-dicarboxylate (**2**), bromobenzene (2.1 g, 20 mmol), **1** (7.25 g, 22 mmol), and K_2CO_3 (36.0 g, 260 mmol) were mixed in 1,4-dioxane (120 mL), and the mixture was purged with argon and stirred for 30 min at room temperature. Then, $Pd(PPh_3)_2Cl_2$ (0.30 g, 0.4 mmol) was added, and the mixture was heated at 65 °C for 24 h under argon. The resultant mixture was extracted with water and $CHCl_3$, and the water phase was then removed. Organic solvent was removed under reduced pressure, and the crude product was purified by column chromatography to obtain pure dimethyl biphenyl-3,5-dicarboxylate (**2**, 4.2 g). Yield: 78%. ^{1}H NMR (500 MHz, $CDCl_3$), δ = 3.99 (s, 6 H), 7.27 (m, 1 H), 7.49 (m, 2 H), 7.67 (t, 2 H), 8.47 (d, 2 H), 8.66 (s, 1 H) ppm. Anal. Calcd for $C_{16}H_{14}O_4$: C, 71.10; H, 5.22. Found: C, 71.24; H, 5.14.

To prepare biphenyl-3,5-dicarboxylate acid (H_2BPDA, **3**), **2** (4.03 g, 14.8 mmol) was suspended in a H_2O (50 mL) solution to which 100 mL of 3 M NaOH aqueous solution had been added. The mixture was stirred under reflux overnight. Dilute HCl was added to the remaining aqueous solution until the solution reached a pH of 2. The solid was collected by filtration, washed with water, and dried to give H_2BPDA (**3**, 3.50 g, 97.5% yield). ^{1}H NMR (500 MHz, DMSO-d_6): δ = 7.47 (t, 1 H), 7.53 (d, 2 H), 7.76 (t, 2 H), 8.38 (d, 2 H), 8.47 (t, 1 H), 13.43 (m, 2 H) ppm. Anal. Calcd for $C_{14}H_{10}O_4$: C, 69.42; H, 4.16. Found: C, 69.64; H, 4.08.

Synthesis of $[Eu(C_{14}H_8O_4)(NO_3)(DMF)_2](DMF)$. A mixture of H_2BPDA (**3**, 24.0 mg, 0.1 mmol) and $Eu(NO_3)_3(H_2O)_6$ (88.0 mg, 0.2 mmol) was dissolved in DMF/dioxane (8 mL, 1:1, v/v) in a screw-capped vial. After acetic acid (40 μL) had been added to the mixture, the vial was capped and placed in an oven at 80 °C for 72 h. The resulting colorless crystals were collected by filtration and washed with DMF several times. Anal. Calcd for $[Eu(C_{14}H_8O_4)(NO_3)(DMF)_2]$-(DMF) ($C_{23}H_{29}N_4O_{10}Cu$, %): C, 41.02; H, 4.34; N, 8.32. Found: C, 40.47; H, 4.25; N, 8.23. IR (KBr, cm^{-1}): 3419 (s), 2932 (m), 1667 (s), 1611 (s), 1589 (s), 1462 (s), 1424 (s), 1384 (s), 1297 (s), 1253 (m), 1114 (s), 1062 (w), 1031 (s), 929 (w), 915 (w), 817 (m), 764 (s), 717 (s), 676 (s), 628 (m), 493 (m). The Tb/Eu mixed MOFs $Tb_{1-x}Eu_x$BPDA (x = 0.005, 0.01, 0.02, 0.05, 0.10, 0.20, 0.50, 0.80) were synthesized similarly to EuBPDA except for the use of mixtures of $Tb(NO_3)_3(H_2O)_6$ and $Eu(NO_3)_3(H_2O)_6$.

RESULTS AND DISCUSSION

A colorless small blocklike crystal of LnBPDA was synthesized by the solvothermal method, namely, the reaction of Ln-$(NO_3)_3{\cdot}6H_2O$ and H_2BPDA in a DMF/dioxane mixture at 80 °C for 3 days. Its formulation was determined to be $[Ln(BPDA)(NO_3)(DMF)_2](DMF)$ (Ln = Gd^{3+}, Eu^{3+}, Tb^{3+}) by TGA, CHN analysis, and single-crystal X-ray diffraction studies. In addition, the same synthetic procedures were used to prepare the M′LnMOFs $Tb_{1-x}Eu_x$BPDA (x = 0.005, 0.01, 0.02, 0.05, 0.10, 0.20, 0.50, 0.80) by varying the original molar ratios $Eu(NO_3)_3$ to $Tb(NO_3)_3$.

Single-crystal X-ray diffraction analysis confirmed that the EuBPDA unit consists of one Eu atom, one BPDA ligand, three DMF molecules, and one NO_3^- ion and crystallizes in the monoclinic space group $P21/c$ (Figure 1 and Table S1, Supporting Information). As shown in Figure 1, the Eu^{3+} ion is

DOI: 10.1021/acs.inorgchem.5b01623
Inorg. Chem. XXXX, XXX, XXX−XXX

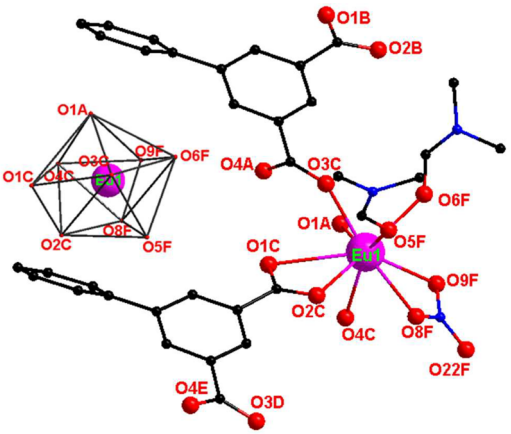

Figure 1. Coordination environment without hydrogen atoms of Eu^{3+} ion. Inset: Coordination polyhedron of Eu^{3+} ion. (Symmetry codes: A, $-x$, $^1/_2 + y$, $^3/_2 - z$; B, x, $1 + y$, $1 + z$; C, x, $^5/_2 - y$, $^3/_2 + z$; D, x, $1 + y$, $2 + z$; E, $-x$, $3 - y$, $2 - z$; F: x, $^5/_2 - y$, $^3/_2 + z$.)

coordinated to nine O atoms, specifically, two from one NO_3^- ion, two from two DMF molecules, and five carboxylate oxygen atoms from four BPDA ligands, and the coordination geometry can be identified as a distorted tricapped trigonal prism. The Eu−O bond lengths range from 2.376 to 2.842 Å. Neighboring Eu^{3+} ions, at a distance of 4.091 Å, are linked by monodentate carbonyl units of the H_2BPDA ligands, consequently forming a dinuclear $Eu_2(COO)_4$ secondary building unit, generating a one-dimensional chain (Figure 2a). The chains are then connected in an orderly fashion to form a two-dimensional layer framework (Figure 2b) of the (4, 4) parallelogram grid topology through the H_2BPDA ligand bridge. Eventually, a condensed three-dimensional structure (Figure 2c) is formed by the two-dimensional layers packed together through weak intermolecular van der Waals interactions and aromatic $\pi-\pi$ interactions. As expected, the LnBPDA MOFs (Tb^{3+}, Eu^{3+}, Gd^{3+}) and the M′LnMOF $Tb_{0.8}Eu_{0.2}$BPDA are isostructural, as confirmed by single-crystal and powder X-ray diffraction analyses (Figure 3). The main crystal structure, which can withstand temperatures of up to 410 °C, was confirmed by the TGA method (Figure S2, Supporting Information), indicating its excellent thermostability.

We are interested in the performance of LnBPDA and $Tb_{1-x}Eu_x$BPDA, as well as their potential for use as luminescent thermometers at physiological temperatures. The excitation and emission spectra of H_2BPDA ligand, TbBPDA, EuBPDA, and $Tb_{1-x}Eu_x$BPDA were recorded at room temperature (Figures S4−S6, Supporting Information). The emission wavelength of ligand H_2BPDA is approximately 365 nm for excitation at 337 nm (Figure S4, Supporting Information). Under irradiation of 323-nm UV light, TbBPDA and EuBPDA displayed typical Tb^{3+} and Eu^{3+} emission peaks, respectively, and $Tb_{1-x}Eu_x$BPDA simultaneously exhibited the characteristic $^5D_4 \rightarrow {}^7F_{6-3}$ (Tb^{3+}) and $^5D_0 \rightarrow {}^7F_{1-4}$ (Eu^{3+}) transitions (Figures S5 and S6, Supporting Information). Interestingly, we could not find the emission bands of the H_2BPDA ligand in the coordination complex, suggesting that the energy-transfer processes from the H_2BPDA ligands to the Tb^{3+} and Eu^{3+} ions are efficient.

We investigated the temperature-dependent photoluminescence (PL) properties of these LnBPDA and $Tb_{1-x}Eu_x$BPDA complexes and characterized them in terms of intensity and

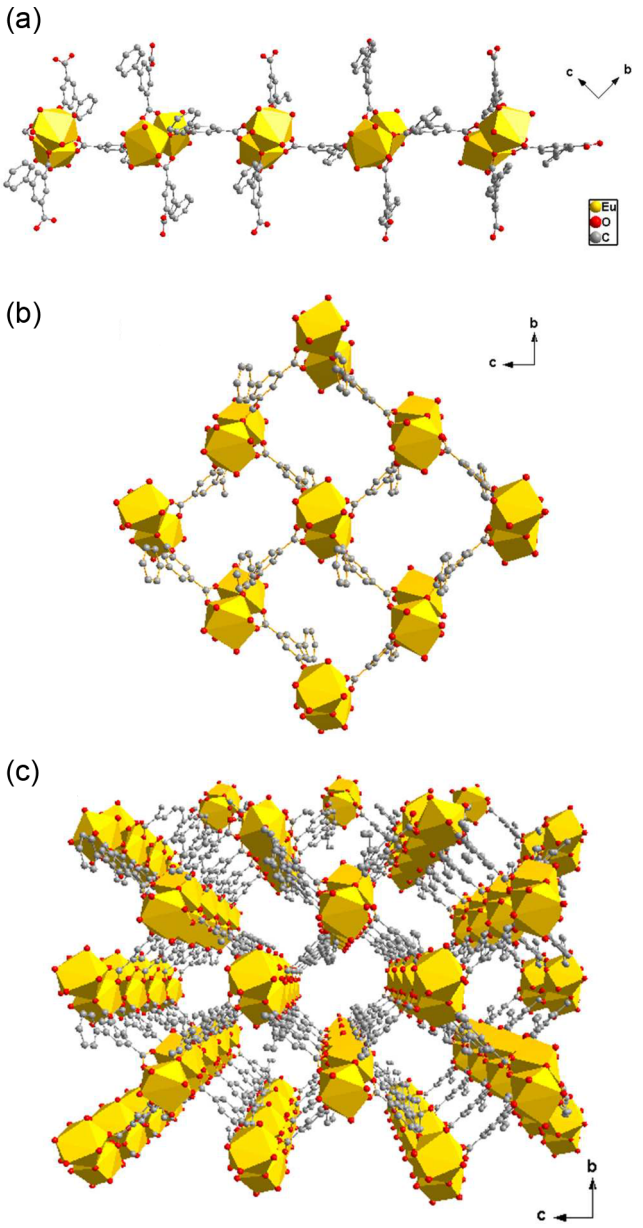

Figure 2. (a) One-dimensional chain structure of EuBPDA along the [100] direction. (b) Two-dimensional layer structure at the (100) plane. (c) Three-dimensional framework packed by weak intermolecular van der Waals interactions and aromatic $\pi-\pi$ interactions along the [100] direction.

lifetime. As shown in Figure S6 (Supporting Information), all of the compounds with different ratios of Tb^{3+} and Eu^{3+} ions exhibited emission spectra with different intensities for Tb^{3+} (544 nm) and Eu^{3+} (614 nm). Usually, the intensity ratio (Tb/Eu) is used as the thermometric parameter to realize temperature sensing, as a proper luminescent intensity ratio between Tb^{3+} and Eu^{3+} is necessary. Obviously, the intensity at 614 nm from $Tb_{0.9}Eu_{0.1}$BPDA is very low, and the intensity at 544 nm from $Tb_{0.5}Eu_{0.5}$BPDA is not noticeable; thus, $Tb_{0.8}Eu_{0.2}$BPDA (where the Tb/Eu ratio was calculated by inductively coupled plasma analysis to be 0.7931:0.2069) is the best sample to be examined in detail. UV light at 323 nm was used to excite $Tb_{0.8}Eu_{0.2}$BPDA in the temperature range from 293 to 328 K, and the temperature-dependent emission spectra are presented in Figure 4a. As expected, the emission intensity

DOI: 10.1021/acs.inorgchem.5b01623
Inorg. Chem. XXXX, XXX, XXX−XXX

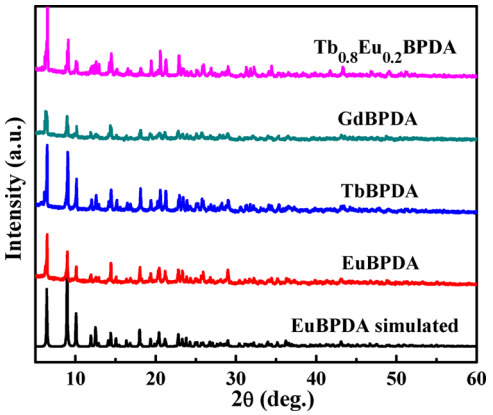

Figure 3. Powder XRD patterns of the LnBPDA units and the M′LnMOF $Tb_{0.8}Eu_{0.2}$BPDA.

of $^5D_0 \rightarrow {}^7F_2$ (Eu^{3+}, 614 nm) increased with temperature, but that of the $^5D_4 \rightarrow {}^7F_5$ (Tb^{3+}, 544 nm) decreased. Figure 4b, which displays the normalized intensities of the corresponding emissions, shows the temperature dependence. The insets of Figure 4b and Figure S7 (Supporting Information) show that the emission intensities of TbBPDA and EuBPDA gradually decreased as the temperature was increased, which can be attributed to thermal activation of nonradiative and mixed-decay transitions.[9c] Thus, the cross-current of the Tb^{3+} and Eu^{3+} ions within $Tb_{0.8}Eu_{0.2}$BPDA can be a typical energy-transfer process where the energy is transferred from the Tb^{3+} ions to the Eu^{3+} ions through a thermally driven phonon-assisted Förster transfer mechanism. This process is quite different from that of $Tb_{0.99}Eu_{0.01}(BDC)_{1.5}(H_2O)_2$,[7e] where the corresponding emission of the Tb^{3+} and Eu^{3+} ions decreases as the temperature increases from 290 to 320 K. That is, the ligand H_2BPDA can efficiently sensitize the Tb^{3+} and Eu^{3+} ions because of a more appropriate energy-level distribution than in 1,4-benzendicarboxylate (H_2BDC).[7e] As can be seen in Table S3 (Supporting Information), the energies of the lowest triplet excited states of H_2BPDA and H_2BDC are 25269 and 26211 cm^{-1}, respectively. These energy levels ensure effective sensitization and efficient energy transfer from the ligands to the Tb^{3+} and Eu^{3+} ions.[5a,9c] A proper distribution of the energy levels for the ligand is crucial for the performance of as-synthesized MOFs because it is closely associated with the intersystem crossing and internal energy conversion in the ligand.[9c] For reference, a schematic of the energy transfer from the ligand to the Tb^{3+} and Eu^{3+} ions is shown in Figure 5. We

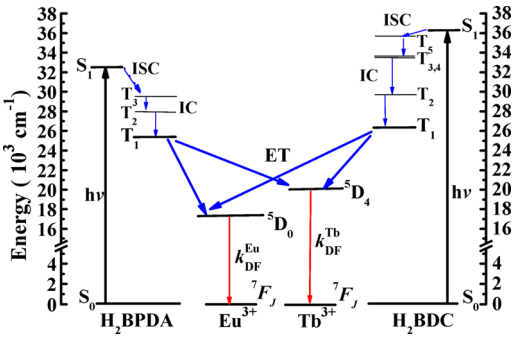

Figure 5. Schematic representation of the energy transfer from the ligand to Tb^{3+} ($^5D_4$) and Eu^{3+} ($^5D_0$) ions. Abbreviations: S, singlet; T, triplet; $h\nu$, energy absorption; ISC, intersystem crossing; ET, energy transfer. Blue and red arrows indicate nonradiative and radiative processes, respectively.

note that H_2BDC has more triplet excited states below the lowest singlet excited state and that they are on higher levels than those of H_2BPDA. This means that, at a given temperature, the effects, including nonradiative decay and relaxation, in the as-synthesized MOF of H_2BDC can be much stronger than that of H_2BPDA. As a result, the sensitization or energy transfer from H_2BPDA to the Tb^{3+} and Eu^{3+} ions is more efficient, so that the luminescence properties of $Tb_{0.8}Eu_{0.2}$BPDA are significantly improved. $Tb_{0.8}Eu_{0.2}$BPDA might therefore be useful for realizing more sensitive and more accurate thermometers for physiological temperature measurements.

It is worth exploring the reason for the sensitivity of $Tb_{0.8}Eu_{0.2}$BPDA being located in the physiological temperature range, which is completely different from other previous materials covering the range from 10 to 300 K.[5a,7c,d] The low-temperature (10−300 K) PL spectra and normalized intensity of $Tb_{0.8}Eu_{0.2}$BPDA were recorded, as shown in Figure 6. Unexpectedly, the characteristic intensities of Tb^{3+} (544 nm) and Eu^{3+} (614 nm) for $Tb_{0.8}Eu_{0.2}$BPDA, which correspond to the $^5D_4 \rightarrow {}^7F_5$ and $^5D_0 \rightarrow {}^7F_2$ transitions, respectively, exhibit an unusual behavior, that is, the intensities of the corresponding

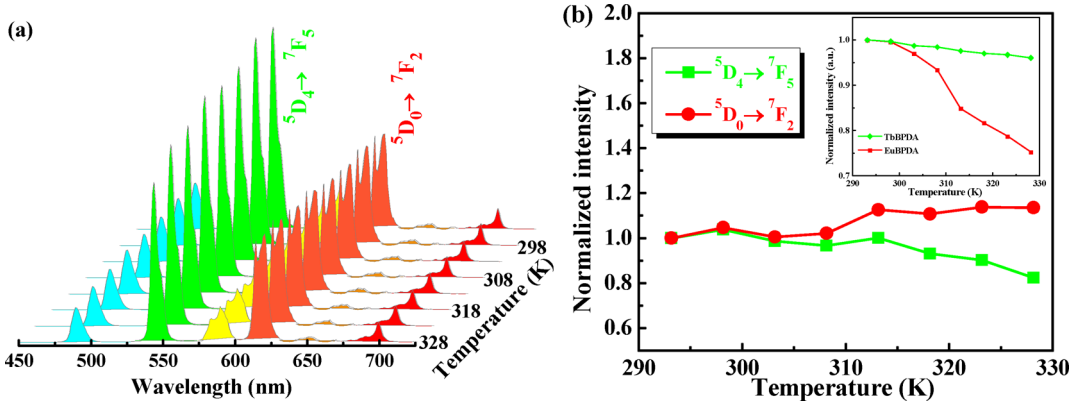

Figure 4. (a) Emission spectra of $Tb_{0.8}Eu_{0.2}$BPDA recorded between 293 and 328 K (excited at 323 nm). (b) Temperature dependence of the normalized intensity of the $^5D_4 \rightarrow {}^7F_5$ and $^5D_0 \rightarrow {}^7F_2$ transitions for $Tb_{0.8}Eu_{0.2}$BPDA. Inset: Temperature-dependent normalized intensities of the $^5D_4 \rightarrow {}^7F_5$ transition of TbBPDA and the $^5D_0 \rightarrow {}^7F_2$ transition of EuBPDA (excited at 323 nm).

DOI: 10.1021/acs.inorgchem.5b01623
Inorg. Chem. XXXX, XXX, XXX−XXX

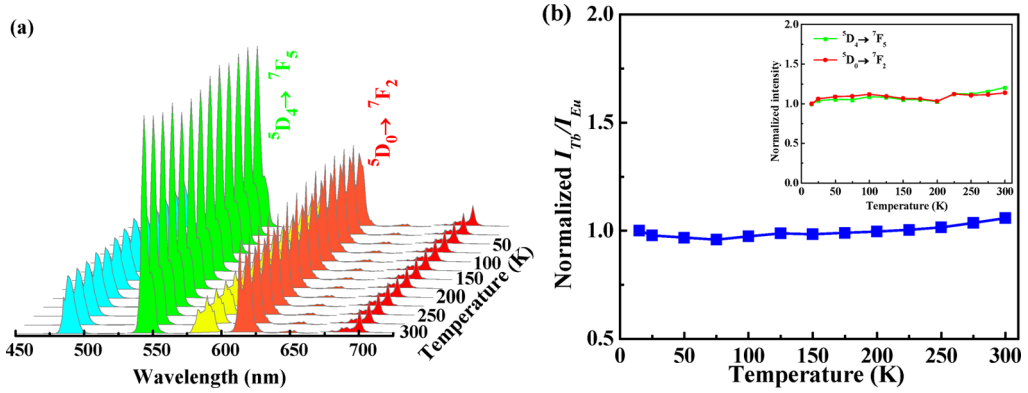

Figure 6. (a) Emission spectra of $Tb_{0.8}Eu_{0.2}$BPDA recorded between 10 and 300 K (excited at 323 nm). (b) Temperature-dependent normalized intensity ratio of $I_{Tb}(^5D_4 \rightarrow {}^7F_5)$ to $I_{Eu}(^5D_0 \rightarrow {}^7F_2)$ for $Tb_{0.8}Eu_{0.2}$BPDA. Inset: Temperature-dependent normalized intensity of the $^5D_4 \rightarrow {}^7F_5$ and $^5D_0 \rightarrow {}^7F_2$ transitions of $Tb_{0.8}Eu_{0.2}$BPDA (excited at 323 nm).

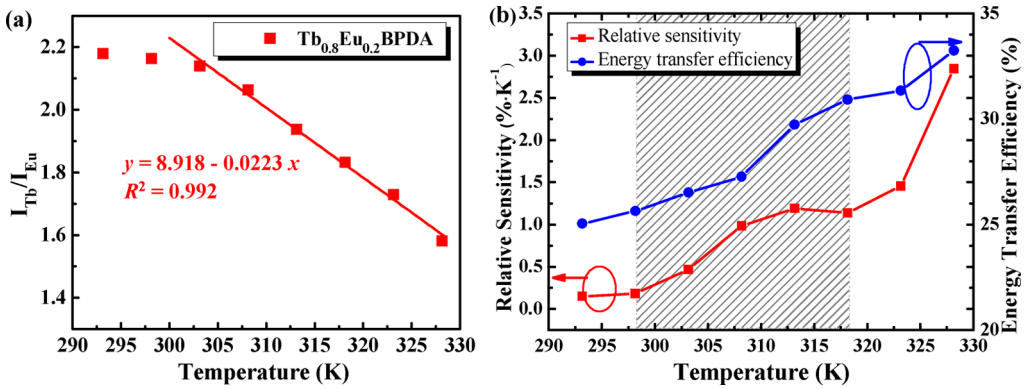

Figure 7. (a) Temperature-dependent intensity ratio of Tb^{3+} (544 nm) to Eu^{3+} (614 nm) and the fitted curve for $Tb_{0.8}Eu_{0.2}$BPDA. (b) Temperature dependence of the relative sensitivity (S_r) and energy-transfer efficiency (η_{ET}) for $Tb_{0.8}Eu_{0.2}$BPDA. The physiological temperature range is shaded.

peaks are very stable even when the temperature increases from 10 to 300 K. As shown and discussed in Figure S8 (Supporting Information), the unusual PL properties of $Tb_{0.8}Eu_{0.2}$BPDA as compared to other samples can be attributed to the sustained and stable highly efficient energy transfer from the ligand to the Tb^{3+} and Eu^{3+} ions in the temperature range from 10 to 300 K. That is, because of the proper energy levels and energy gaps among the singlet and triplet excited states of the H_2BPDA ligand, nonradiative decay or relaxation and energy back-transfer are not strong enough to affect the sensitization in $Tb_{0.8}Eu_{0.2}$BPDA. This is a precondition for the excellent performance of $Tb_{0.8}Eu_{0.2}$BPDA above room temperature, specifically, in the range of physiological temperatures.

The intensity ratio of two different emissions (I_{Tb}/I_{Eu}) is generally used as the thermometric parameter in ratiometric luminescent thermometers, because it has the distinct advantage of being independent of the sensor concentrations in the medium and being a self-calibrating measurement of the temperature from the emission spectra. As shown in Figure 7a, the intensity ratio Δ [$\Delta = I_{Tb}/I_{Eu}$, where I_{Tb} and I_{Eu} are the emission intensities of the $^5D_4 \rightarrow {}^7F_5$ (Tb^{3+} at 544 nm) and $^5D_0 \rightarrow {}^7F_2$ (Eu^{3+} at 614 nm) transitions, respectively] of $Tb_{0.8}Eu_{0.2}$BPDA as a function of temperature shows a good linear relationship in the range from 303 to 328 K that can be fitted as a linear function with a correlation coefficient of R^2 = 0.992 and expressed as

$$\Delta = 8.918 - 0.0223T \quad (1)$$

where T is the given temperature. Thus, this plot indicates $Tb_{0.8}Eu_{0.2}$BPDA is an excellent luminescent thermometer in the range from 303 to 328 K. Furthermore, the emission spectra of $Tb_{0.9}Eu_{0.1}$BPDA and $Tb_{0.5}Eu_{0.5}$BPDA were recorded to evaluate the effects of the amounts of lanthanide ions in the M′LnMOF. As can be seen in Figures S9 and S10 (Supporting Information), the intensity ratios (Δ) for the two MOFs increased with temperature until approximately 293 K and then decreased and exhibited linear relationships in the range of 293−328 K. However, they are not ideal luminescent sensors because Δ changes only slightly compared to that of $Tb_{0.8}Eu_{0.8}$BPDA in the physiological temperature range (Figure S11, Supporting Information). Thus, the PL performance of $Tb_{1-x}Eu_x$BPDA at low temperatures can be tuned by varying the original molar ratios of $Tb(NO_3)_3$ and $Eu(NO_3)_3$, an approach that can be useful in the design of luminescent thermometers.

For comparison with other system reported in the literature and verification of the performance of the new M′MOF $Tb_{0.8}Eu_{0.2}$BPDA, the generalized relative sensitivity (S_r) was determined[5c]

$$S_r = \frac{(\partial\Delta/\partial T)}{\Delta} \quad (2)$$

where T represents the temperature. The evolution of the relative sensitivity S_r with temperature is presented in Figure 7b. One can see that, in the shaded area, which represents the physiological temperature range (298−318 K), the maximum

DOI: 10.1021/acs.inorgchem.5b01623
Inorg. Chem. XXXX, XXX, XXX−XXX

value of S_r for $Tb_{0.8}Eu_{0.2}$BPDA is 1.19%/K at approximately 313 K, which is 7.5 times larger than that of the M′LnMOF ratiometric luminescent thermometer $Tb_{0.99}Eu_{0.01}(BDC)_{1.5}(H_2O)_2$ reported by Cadiau et al.[7e] Thus, it is more advantageous as a candidate for application as a luminescent thermometer because of its high sensitivity.

In addition, another critical characteristic of M′MOFs is the fluorescence lifetime, which refers to the average time that a molecule stays in its excited state before emitting a photon. As shown in Figure S12 (Supporting Information), Ln(Tb,Eu)-BPDA and $Tb_{0.8}Eu_{0.2}$BPDA exhibit different fluorescence lifetimes and special features. One can see that $Tb_{0.8}Eu_{0.2}$BPDA has a shorter $^5D_4(Tb^{3+})$ lifetime than TbBPDA but a longer $^5D_0(Eu^{3+})$ lifetime than EuBPDA from 293 to 328 K. Furthermore, the lifetime of $^5D_4$ in $Tb_{0.8}Eu_{0.2}$BPDA decreases gradually with temperature, whereas the lifetime of $^5D_4$ in TbBPDA tends to be stable. All of these phenomena also indicate that energy transfer from Tb^{3+} to Eu^{3+} occurs when the temperature is increased. It should be noted that the lifetime of $Tb_{0.8}Eu_{0.2}$BPDA is longer than those of existing M′MOFs[5a,7d] and that both the Tb^{3+} signal of TbBPDA and the Eu^{3+} signal of EuBPDA remain stable without decay as the temperature is increased, in stark contrast to the behavior of existing M′MOFs.[5a,7d] As shown in Figure S13 (Supporting Information), the rare-earth ions can be sensitized efficiently by H_2BPDA ligands even at higher temperatures.

We now consider the energy-transfer process from Tb^{3+} to Eu^{3+} in $Tb_{0.8}Eu_{0.2}$BPDA. The efficiency (η_{ET}) of energy transfer from Tb^{3+} to Eu^{3+} can be estimated from the equation[16]

$$\eta_{ET} = \frac{\tau_1^{-1} - \tau_0^{-1}}{\tau_1^{-1}} \quad (3)$$

where τ_0 and τ_1 are the luminescence lifetimes of the $^5D_4$ emission of Tb^{3+} at 544 nm in TbBPDA and $Tb_{0.8}Eu_{0.2}$BPDA, respectively. Figure 7b shows that η_{ET} increases stably with temperature. The energy transfer is thus efficient, and the enhancement of the emission intensity of Eu^{3+} with temperature occurs is at the cost of quenching the Tb^{3+} emission.

The emission of $Tb_{0.8}Eu_{0.2}$BPDA is illustrated by the CIE (Commission Internationale de L'Eclairage) chromaticity diagram coordinates, shown in Figure S14 (Supporting Information). Apparently, the light can be clearly and directly observed by the naked eye and camera. That is, the color can be systematically tuned from yellow to yellow-red from 393 to 328 K, as the corresponding CIE coordinates change from (0.4343, 0.5179) at 393 K to (0.4708, 0.4905) at 328 K. Therefore, $Tb_{0.8}Eu_{0.2}$BPDA is useful as a sensitive luminescent colorimetric thermometer for in situ visualization in the physiological temperature range.

CONCLUSIONS

In summary, the organic ligand biphenyl-3,5-dicarboxylic acid was selected for the synthesis of the new mixed-lanthanide metal−organic framework $Tb_{0.8}Eu_{0.2}$BPDA, because its suitable distribution of energy levels (singlet and triplet excited states) can effectively sensitize the Tb^{3+} and Eu^{3+} ions to generate light emission and because its crystal structure is both thermostable and rigid, as confirmed by TGA and PXRD, respectively. The potential application of $Tb_{0.8}Eu_{0.2}$BPDA as a ratiometric luminescent thermometer operating in the physiological temperature range was evaluated and discussed in detail in terms of fluorescence intensity and lifetime. The fluorescence intensity and lifetime properties of $Tb_{0.8}Eu_{0.2}$BPDA were compare with those of previously reported M′LnMOFs. The temperature dependence of the intensity ratio of two emissions (I_{Tb}/I_{Eu}) can used as the ratiometric thermometric parameter, with no need for any additional calibration of luminescence intensity in real applications. The sensitivity of $Tb_{0.8}Eu_{0.2}$BPDA is clearly higher than those of previously reported M′LnMOFs and is sufficient to satisfy the precision of thermometers used in measurements at physiological temperatures.

This study therefore provides a guide for designing M′LnMOF thermometers with fast responses and high sensitivities in the physiological temperature range that could be useful for intracellular sensing and thermal mapping in biological systems.

ASSOCIATED CONTENT

Supporting Information

Supporting Information for this article is available free of charge via the Internet at The Supporting Information is available free of charge on the ACS Publications website at DOI: 10.1021/acs.inorgchem.5b01623.

Crystallographic data collection and refinement result for EuBPDA; quantum yields of LnBPDA and $Tb_{1-x}Eu_x$BPDA at room temperature; powder XRD patterns of EuBPDA; TGA curves of LnBPDA under nitrogen; FTIR spectrum of $Tb_{0.8}Eu_{0.2}$BPDA; excitation and emission spectra of the H_2BPDA ligand, TbBPDA, and EuBPDA at room temperature; emission spectra and CIE chromaticity diagram of $Tb_{1-x}Eu_x$BPDA upon excitation at 323 nm at room temperature (x = 0, 0.005, 0.01, 0.02, 0.05, 0.10, 0.20, 0.50, 0.80, 1.0); emission spectra of TbBPDA and EuBPDA between 293 and 328 K (excited at 323 nm); temperature dependence of the normalized intensity of the $^5D_4 \rightarrow {}^7F_5$ and $^5D_0 \rightarrow {}^7F_2$ transitions and temperature-dependent normalized intensity ratios of $I_{Tb}(^5D_4 \rightarrow {}^7F_5)$ to $I_{Eu}(^5D_0 \rightarrow {}^7F_2)$ for $Tb_{0.8}Eu_{0.2}$BPDA, $Tb_{0.9}Eu_{0.1}$PIA, $Tb_{0.0069}Eu_{0.9931}$DMBDC, and $Tb_{0.0957}Eu_{0.0043}$CPDA; emission spectra recorded between 10 and 328 K (excited at 323 nm) for $Tb_{0.9}Eu_{0.1}$BPDA and $Tb_{0.5}Eu_{0.5}$BPDA and corresponding temperature-dependent normalized intensity ratios of Tb ($^5D_4 \rightarrow {}^7F_5$) and Eu ($^5D_0 \rightarrow {}^7F_2$); temperature-dependent intensity ratios of Tb3+ (544 nm) to Eu3+ (614 nm) for $Tb_{0.8}Eu_{0.2}$BPDA, $Tb_{0.9}Eu_{0.1}$BPDA, and $Tb_{0.5}Eu_{0.5}$BPDA; temperature dependence of the $^5D_4$ lifetime for TbBPDA, the $^5D_0$ lifetime for EuBPDA, and both lifetimes for $Tb_{0.8}Eu_{0.2}$BPDA and lifetimes of the emission of the corresponding MOFs; temperature-dependent normalized lifetime ratios $[\tau_{Tb}(^5D_4)/\tau_{Eu}(^5D_0)]$ for $Tb_{0.8}Eu_{0.2}$BPDA, $Tb_{0.9}Eu_{0.1}$PIA, and $Tb_{0.0069}Eu_{0.9931}$DMBDC in the temperature range from 10 to 300 K; CIE chromaticity coordinates of $Tb_{0.8}Eu_{0.2}$BPDA recorded between 293 and 328 K (excited at 323 nm); calculated excited-state and HOMO−LUMO energy levels of ligands; optimized geometries of the free ligands H_2BPDA and H_2BDC at the B3LYP/6- 31+G(d,p) level (PDF)

CIF data for $C_{23}H_{29}N_4O_{10}Eu$ (CIF)

AUTHOR INFORMATION

Corresponding Authors

*E-mail: cuiyj@zju.edu.cn (Y.C.).

DOI: 10.1021/acs.inorgchem.5b01623
Inorg. Chem. XXXX, XXX, XXX−XXX

*E-mail: gdqian@zju.edu.cn (G.Q.).

Author Contributions

The manuscript has been discussed and commented by all authors.

Notes

The authors declare no competing financial interest.

■ ACKNOWLEDGMENTS

This work was supported by the National Natural Science Foundation of China (Nos. 51272229, 51272231, 51402259, 51472217, and 51432001), Zhejiang Provincial Natural Science Foundation of China (Nos. LR13E020001 and LZ15E020001), Qianjiang Talent Project (No. QJD1302009), and Fundamental Research Funds for the Central Universities (Nos. 2015QNA4009, 2015FZA4008, and 2014XZZX005).

■ REFERENCES

(1) (a) Brites, C. D. S.; Lima, P. P.; Silva, N. J. O.; Millan, A.; Amaral, V. S.; Palacio, F.; Carlos, L. D. *New J. Chem.* **2011**, *35*, 1177−1183. (b) Uchiyama, S.; de Silva, A. P.; Iwai, K. *J. Chem. Educ.* **2006**, *83*, 720−727. (c) Feng, J.; Tian, K.; Hu, D.; Wang, S.; Li, S.; Zeng, Y.; Li, Y.; Yang, G. *Angew. Chem., Int. Ed.* **2011**, *50*, 8072−8076.

(2) Cauzzi, D.; Pattacini, R.; Delferro, M.; Dini, F.; Di Natale, C.; Paolesse, R.; Bonacchi, S.; Montalti, M.; Zaccheroni, N.; Calvaresi, M.; Zerbetto, F.; Prodi, L. *Angew. Chem., Int. Ed.* **2012**, *51*, 9662−9665.

(3) (a) Sun, L. N.; Yu, J.; Peng, H.; Zhang, J. Z.; Shi, L.-Y.; Wolfbeis, O. S. *J. Phys. Chem. C* **2010**, *114*, 12642−12648. (b) Feng, P. L.; Leong, K.; Allendorf, M. D. *Dalton Trans.* **2012**, *41*, 8869−8877. (c) Jaque, D.; Vetrone, F. *Nanoscale* **2012**, *4*, 4301−4326.

(4) Haro-González, P.; Martínez-Maestro, L.; Martín, I. R.; García-Solé, J.; Jaque, D. *Small* **2012**, *8*, 2652−2658.

(5) (a) Cui, Y.; Xu, H.; Yue, Y.; Guo, Z.; Yu, J.; Chen, Z.; Gao, J.; Yang, Y.; Qian, G.; Chen, B. *J. Am. Chem. Soc.* **2012**, *134*, 3979−3982. (b) Carlos, L. D.; Ferreira, R. A. S.; de Zea Bermudez, V.; Julian-Lopez, B.; Escribano, P. *Chem. Soc. Rev.* **2011**, *40*, 536−549. (c) Cui, Y.; Zhu, F.; Chen, B.; Qian, G. *Chem. Commun.* **2015**, *51*, 7420−7431. (d) Cui, Y.; Song, R.; Yu, J.; Liu, M.; Wang, Z.; Wu, C.; Yang, Y.; Wang, Z.-Y.; Chen, B.; Qian, G. *Adv. Mater.* **2015**, *27*, 1420−1425.

(6) (a) Vetrone, F.; Naccache, R.; Zamarrón, A.; Juarranz de la Fuente, A.; Sanz-Rodríguez, F.; Martinez Maestro, L.; Martín Rodriguez, E.; Jaque, D.; García Solé, J.; Capobianco, J. A. *ACS Nano* **2010**, *4*, 3254−3258. (b) Brites, C. D. S.; Lima, P. P.; Silva, N. J. O.; Millan, A.; Amaral, V. S.; Palacio, F.; Carlos, L. D. *Adv. Mater.* **2010**, *22*, 4499−4504. (c) Sedlmeier, A.; Achatz, D. E. D. E.; Fischer, L. H.; Gorris, H. H.; Wolfbeis, O. S. *Nanoscale* **2012**, *4*, 7090−7096. (d) Lee, J.; Govorov, A. O.; Kotov, A. N. *Angew. Chem., Int. Ed.* **2005**, *44*, 7439−7442. (e) Chen, C. Y.; Chen, C. T. *Chem. Commun.* **2011**, *47*, 994−996. (f) Wu, C.; Schneider, T.; Zeigler, M.; Yu, J.; Schiro, P. G.; Burnham, D. R.; McNeill, J. D.; Chiu, D. T. *J. Am. Chem. Soc.* **2010**, *132*, 15410−15417. (g) Ye, F. M.; Wu, C. F.; Jin, Y. H.; Chan, Y. H.; Zhang, X. J.; Chiu, D. T. *J. Am. Chem. Soc.* **2011**, *133*, 8146−8149.

(7) (a) Miyata, K.; Konno, Y.; Nakanishi, T.; Kobayashi, A.; Kato, M.; Fushimi, K.; Hasegawa, Y. *Angew. Chem., Int. Ed.* **2013**, *52*, 6413−6416. (b) Ma, D.; Li, B.; Zhou, X.; Zhou, Q.; Liu, K.; Zeng, G.; Li, G.; Shi, Z.; Feng, S. *Chem. Commun.* **2013**, *49*, 8964−8966. (c) Cui, Y.; Zou, W.; Song, R.; Yu, J.; Zhang, W.; Yang, Y.; Qian, G. *Chem. Commun.* **2014**, *50*, 719−721. (d) Rao, X.; Song, T.; Gao, J.; Cui, Y.; Yang, Y.; Wu, C.; Chen, B.; Qian, G. *J. Am. Chem. Soc.* **2013**, *135*, 15559−15564. (e) Cadiau, A.; Brites, C. D. S.; Costa, P. M. F. J.; Ferreira, R. A. S.; Rocha, J.; Carlos, L. D. *ACS Nano* **2013**, *7*, 7213−7218. (f) Zhang, J.; Zhang, H.; Du, Z.; Wang, X.; Yu, S.; Jiang, H. *Chem. Commun.* **2014**, *50*, 1092−1094. (g) Zhang, H.; Zhang, J.; Huang, G.; Du, Z.; Jiang, H. *Chem. Commun.* **2014**, *50*, 12069−12072.

(8) (a) Rocha, J.; Carlos, L. D.; Paz, F. A. A.; Ananias, D. *Chem. Soc. Rev.* **2011**, *40*, 926−940. (b) Chen, B.; Xiang, S.; Qian, G. *Acc. Chem. Res.* **2010**, *43*, 1115−1124. (c) Lu, W.; Wei, Z.; Gu, Z.-Y.; Liu, T.-F.; Park, J.; Park, J.; Tian, J.; Zhang, M.; Zhang, Q.; Gentle, T., III; Bosch, M.; Zhou, H.-C. *Chem. Soc. Rev.* **2014**, *43*, 5561−5593. (d) Makal, T. A.; Li, J.-R.; Lu, W.; Zhou, H.-C. *Chem. Soc. Rev.* **2012**, *41*, 7761−7779.

(9) (a) Cui, Y.; Yue, Y.; Qian, G.; Chen, B. *Chem. Rev.* **2012**, *112*, 1126−1162. (b) Binnemans, K. *Chem. Rev.* **2009**, *109*, 4283−4374. (c) Armelao, L.; Quici, S.; Barigelletti, F.; Accorsi, G.; Bottaro, G.; Cavazzini, M.; Tondello, E. *Coord. Chem. Rev.* **2010**, *254*, 487−505. (d) Cui, Y.; Chen, B.; Qian, G. *Coord. Chem. Rev.* **2014**, *273-274*, 76−86. (e) Hu, Z.; Deibert, B. J.; Li, J. *Chem. Soc. Rev.* **2014**, *43*, 5815−5840.

(10) *CrysAlisPro*, version 1.171.33.56; Oxford Diffraction Ltd.: Oxfordshire, U.K., 2010.

(11) Sheldrick G. M. *SHELXL-97: Program for the Refinement of Crystal Structures*; University of Göttingen: Göttingen, Germany, 1997.

(12) Becke, A. D. *J. Chem. Phys.* **1993**, *98*, 5648−5652.

(13) Runge, E.; Gross, E. K. U. *Phys. Rev. Lett.* **1984**, *52*, 997−1000.

(14) Frisch, M. J.; Trucks, G. W.; Schlegel, H. B.; Scuseria, G. E.; Robb, M. A.; Cheeseman, J. R.; Scalmani, G.; Barone, V.; Mennucci, B.; Petersson, G. A.; Nakatsuji, H.; Caricato, M.; Li, X.; Hratchian, H. P.; Izmaylov, A. F.; Bloino, J.; Zheng, G.; Sonnenberg, J. L.; Hada, M.; Ehara, M.; Toyota, K.; Fukuda, R.; Hasegawa, J.; Ishida, M.; Nakajima, T.; Honda, Y.; Kitao, O.; Nakai, H.; Vreven, T.; Montgomery, J. A., Jr.; Peralta, J. E.; Ogliaro, F.; Bearpark, M.; Heyd, J. J.; Brothers, E.; Kudin, K. N.; Staroverov, V. N.; Keith, T.; Kobayashi, R.; Normand, J.; Raghavachari, K.; Rendell, A.; Burant, J. C.; Iyengar, S. S.; Tomasi, J.; Cossi, M.; Rega, N.; Millam, J. M.; Klene, M.; Knox, J. E.; Cross, J. B.; Bakken, V.; Adamo, C.; Jaramillo, J.; Gomperts, R.; Stratmann, R. E.; Yazyev, O.; Austin, A. J.; Cammi, R.; Pomelli, C.; Ochterski, J. W.; Martin, R. L.; Morokuma, K.; Zakrzewski, V. G.; Voth, G. A.; Salvador, P.; Dannenberg, J. J.; Dapprich, S.; Daniels, A. D.; Farkas, Ö.; Foresman, J. B.; Ortiz, J. V.; Cioslowski, J.; Fox, D. J. *Gaussian 09*, revision D.01; Gaussian Inc.: Pittsburgh, PA, 2009.

(15) Chen, Z.; Xiang, S.; Liao, T.; Yang, Y.; Chen, Y.; Zhou, M.; Zhao, D.; Chen, B. *Cryst. Growth Des.* **2010**, *10*, 2775−2779.

(16) Rodrigues, M. O.; Dutra, J. D. L.; Nunes, L. A. O.; de Sá, G. F.; de Azevedo, W. M.; Silva, P.; Paz, F. A. A.; Freire, R. O.; Júnior, S. A. *J. Phys. Chem. C* **2012**, *116*, 19951−19957.

DOI: 10.1021/acs.inorgchem.5b01623
Inorg. Chem. XXXX, XXX, XXX−XXX